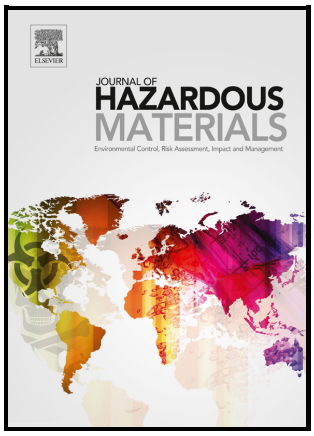

Bisphenol A Degradation by Manganese Oxides at Circumneutral pH: Quantitative Evaluation of Dissolved Mn(III) Species with Pyrophosphate

Xiaohan Lu, Xingxing Wang, Haohua He, Qiuyao Liu, Jinfeng Li, Ziyi Zhao, Peng Yang, Zezhen Pan, Zimeng Wang

PII: S0304-3894(24)03594-5

DOI: https://doi.org/10.1016/j.jhazmat.2024.137013

Reference: HAZMAT137013

To appear in: *Journal of Hazardous Materials*

Received date: 1 August 2024
Revised date: 9 December 2024
Accepted date: 24 December 2024

Please cite this article as: Xiaohan Lu, Xingxing Wang, Haohua He, Qiuyao Liu, Jinfeng Li, Ziyi Zhao, Peng Yang, Zezhen Pan and Zimeng Wang, Bisphenol A Degradation by Manganese Oxides at Circumneutral pH: Quantitative Evaluation of Dissolved Mn(III) Species with Pyrophosphate, *Journal of Hazardous Materials,* (2024) doi:https://doi.org/10.1016/j.jhazmat.2024.137013

Bisphenol A Degradation by Manganese Oxides at Circumneutral pH: Quantitative Evaluation of Dissolved Mn(III) Species with Pyrophosphate

Xiaohan Lu [a], Xingxing Wang [b, a]*, Haohua He [a], Qiuyao Liu [a], Jinfeng Li [a], Ziyi Zhao [a], Peng Yang [c], Zezhen Pan [a, d], , Zimeng Wang [a, d, e, f]*

[a] Department of Environmental Science and Engineering, Fudan University, Shanghai 200433, China

[b] School of Environmental Science and Engineering, Southern University of Science and Technology, Shenzhen 518055, China.

[c] Chemical Sciences Division, Oak Ridge National Laboratory, Oak Ridge, Tennessee 37831, United States

[d] National Observations and Research Station for Wetland Ecosystems of the Yangtze Estuary, Institute of Eco-Chongming, Fudan University, Shanghai 200062, China

[e] Institute of Atmospheric Sciences, Fudan University, Shanghai 200438, China

[f] Shanghai Institute of Pollution Control and Ecological Security, Shanghai 200092, China

*Corresponding author: xingxingwang12@outlook.com, wangxx3@sustech.edu.cn;

zimengw@fudan.edu.cn

Manuscript Submitted to

Journal of Hazardous Materials

Abstract

Although trivalent manganese (Mn(III)) species have been recognized as crucial intermediates in the degradation of organic contaminants by Mn oxides, quantitative research on their specific roles remains scarce. Our study investigated the degradation processes of an organic pollutant, Bisphenol A (BPA), by dissolved Mn(III) and Mn(III)-bearing oxides, and elucidated the differences of the underlying mechanisms and reaction pathways between several Mn oxides and dissolved Mn(III). Our results indicated that BPA degradation rates with Mn(III)-bearing oxides alone follow the order: δ-MnO_2 ≫ γ-MnOOH > Mn_3O_4. Adding pyrophosphate (PP) significantly enhanced BPA degradation by promoting the formation of Mn(III)-PP complexes and

exposing more reactive sites, achieved through destabilizing the crystal structure and mitigating of Mn(II) readsorption, particularly in γ-MnOOH and Mn_3O_4. Our kinetic model revealed that heterogeneous degradation by Mn oxides is the predominant reaction pathway, accounting for 61.4%, 87.8%, and 73.8% of the total degraded BPA for δ-MnO_2, γ-MnOOH, and Mn_3O_4, respectively, even in the presence of significant amount of dissolved Mn(III) intermediates due to high PP concentrations. These results offer mechanistic details on BPA degradation by Mn oxides and the influence of ligand concentration, providing helpful insights for optimizing degradation strategies of organic pollutants.

Keywords:

dissolved Mn(III), Bisphenol A, pyrophosphate, manganese oxides, kinetic modeling

Environmental Implications

This study shows that different Mn oxides and dissolved Mn(III) species significantly affect the degradation of Bisphenol A (BPA), a pollutant with estrogenic toxicity. The presence of pyrophosphate (PP) enhances degradation, suggesting that specific soil ligands can boost the natural breakdown of contaminants. By forming Mn(III)-PP complexes and reducing surface passivation, PP and similar compounds can increase pollutant degradation efficiency in soil and water. These findings improve our understanding of degradation mechanisms in natural environments and offer practical applications for enhancing natural attenuation processes, contributing to better environmental management and public health protection.

1. Introduction

Manganese (Mn), ranked as the third most abundant transition metal in the earth's crust, primarily exists in II, III, and IV oxidation states within soils and sediments. The substantial surface area and high redox potential of Mn oxides endow them with a significant influence on biogeochemical processes in various environments, surpassing their relative natural abundance [1, 2]. Previous research has primarily focused on the stable forms of Mn, specifically the soluble Mn(II) and the insoluble Mn(IV), while neglecting the less stable Mn(III) species [3, 4]. Increasingly, studies are demonstrating that dissolved Mn(III) species ($Mn(III)_{(aq)}$) are crucial for the reaction dynamics between Mn and organic compounds [5-7]. The presence of Mn(III) within natural Mn(III/IV) oxides has been found to reduce their overall oxidizing capability, potentially obstructing the degradation process [8, 9]. Meanwhile, dissolved Mn(III) displays faster ligand exchange rates and possesses

a higher redox potential ($E_H^\circ(Mn^{3+}/Mn^{2+})$=1.51 V) than solid Mn(IV) ($E_H^\circ(MnO_2/Mn^{2+})$=1.23 V) [10, 11], which results in a faster oxidation rate of organic matter compared to systems containing only solid Mn oxides. However, a comprehensive understanding of the critical role of Mn(III) in the oxidative decomposition of organic carbon by Mn oxides, both in its dissolved form and as a part of solid mineral structures remain to be explored.

Furthermore, in the presence of natural organic ligands (L), the formation and presence of Mn(III)-L complexes would significantly affect the interactions between Mn oxides and organic carbon [12, 13]. Pyrophosphate (PP), found ubiquitously in various environmental settings such as in marine waters and sediments [14, 15], and anthropogenic discharges [16], is a model ligand in Mn(III) studies due to its ability to stabilize Mn(III) in the form of dissolved Mn(III)-PP complexes [17]. Interestingly, previous research has shown contrasting effects of PP on the behavior of Mn(III) as an oxidizing agent. PP was reported to complex with reactive surficial Mn(III), and exerted an inhibitory effect on the oxidation of Cr(III), sulfide and phenol by δ-MnO_2 [18, 19]. Conversely, PP also enhanced the oxidative disintegration of organic contaminants (e.g. Bisphenol A (BPA)) by Mn oxides through the formation of Mn(III)-PP complexes, which actively participated in the disintegration process [20, 21]. The degradation of BPA by Mn oxides has been extensively studied, with a primary focus on MnO_2 [20-23]. Furthermore, prior research indicated that at excessively high concentrations, PP might paradoxically inhibit the oxidative capacity of the Mn(III)-PP complexes, suggesting a dual-regime role of ligands in modulating the redox behavior of Mn(III) [24]. Therefore, though the effect of dissolved Mn(III) intermediates and the concentration of PP on the degradation of environmentally concerning pollutants have been studied, the quantitative contribution of dissolved Mn(III) species to the overall degradation of pollutants by Mn oxide has remained underexplored.

Here, BPA, a common organic pollutant detected in soil and underground water from industrial discharges [25, 26], was selected to understand the underlying mechanisms of its degradation by dissolved Mn(III)-PP complexes and three Mn(III)-bearing oxides, δ-MnO_2, γ-MnOOH, and Mn_3O_4. These three Mn oxides were chosen because they represent distinct structural and redox characteristics of Mn(III)-bearing oxides, making them representative of the broader Mn oxide family. The main objectives were: (1) to unravel the differences in reaction mechanisms through which Mn oxides of varied valence states facilitate the degradation of BPA and to quantify the contributions of various pathways; and (2) to examine the role of PP as a model ligand and

the effect of PP concentration in the degradation of BPA by these Mn oxides. With a combination of wet chemistry techniques, spectroscopic analysis, and kinetic modeling approaches, our research explored how PP concentrations influenced BPA degradation by Mn oxides and the pivotal role of intermediate Mn(III) species in this context. These results highlighted the complex interactions and dynamics within various environments, offering potential strategies for enhancing the natural remediation of organic pollutants such as BPA.

2. Materials and Methods

2.1 Sample Preparation and Batch Experiments

Three Mn(III)-containing minerals, birnessite (δ-MnO_2), manganite (γ-MnOOH), and hausmannite (Mn_3O_4), and the dissolved Mn(III)-PP complexes were used to study the interaction between Mn(III) species and BPA. Four distinct batch experiments were conducted (as summarized in Table 1) to evaluate the influence of PP concentration on BPA degradation by Mn(III)-containing species: (1) dissolved Mn(III)-PP complexes; (2) δ-MnO_2; (3) γ-MnOOH; (4) Mn_3O_4.

Desired PP:Mn ratios were achieved by adding specific volumes of a 100 mM PP stock solution to deionized water. A 20 mM 4-morpholinepropanesulfonic acid (MOPS) was used as a pH buffer to maintain the pH at 7.0. To ensure homogeneity in reactions, BPA and PP were introduced at least 12 hours prior to the addition of the Mn(III)-PP stock solution and the Mn minerals. No significant degradation of BPA was observed during this period. More detailed information about the batch experiments was provided in Supporting Information (SI).

2.2 Analysis Methods

For the assessment of BPA degradation, 2 mL aliquots were sampled at predetermined intervals and filtered through 0.22 μm poly(ether sulfone) (PES) syringe filters. The samples were analyzed using High-Performance Liquid Chromatography (HPLC, LC: 1290 Infinity II with Zorbax SB-Aq Columns, Agilent, USA) equipped with a variable wavelength ultraviolet detector. Dissolved Mn(III), generated during the reaction between BPA and Mn oxides, was captured by rapidly introducing the filtered solution sample into a 0.1 M PP solution. This mixture aimed to stabilize Mn(III) species to prevent further reactions with BPA [27]. The solution was then analyzed using UV-vis spectrophotometry (Cary 60, Agilent, USA) at 258 nm, following established protocols [11, 28, 29]. Further methodological details were provided in the SI.

3. Results

3.1 BPA Degradation in the Presence of Mn(III)-PP Complexes

In this study, three initial Mn(III) concentrations (100, 300, and 600 μM) were tested to assess their effect on BPA degradation at pH 7.0 (Table 1). For each concentration of dissolved Mn(III), PP was added in both 6-fold and 20-fold molar excess. Preliminary experiments indicated that BPA remained stable (~ 100 μM) in the presence of only 3 mM PP under ambient atmospheric conditions for at least 24 hours. In the 6-fold excess experiments, rapid degradation of BPA was observed within the initial 10 minutes, followed by a slowdown in the reaction rates (Figure 1a). After a 2-hour reaction, the reduction percentages of the initial BPA by 100, 300, and 600 μM Mn(III) were 41%, 57%, and 55%, respectively (Figure 1a). In the 20-fold excess experiments, BPA degradation followed second-order kinetics in the first 45 minutes of the process but later exhibited a similar deceleration, except at the highest PP concentration (12000 μM). After 2 hours, 22%, 20%, and 14% of the initial BPA were degraded at respective Mn(III) concentrations. The second-order rate constants (k) for the 20-fold experiments, calculated from early time points where a linear relationship was observed, were 1.2×10^{-4}, 2.6×10^{-5}, and 1.4×10^{-5} μM^{-1} min^{-1} (Table 1). The results highlighted two primary trends: (1) higher initial Mn(III) concentrations enhanced BPA removal; (2) increased PP concentration at a constant Mn(III) level reduced the degradation efficiency of BPA. Notably, while increasing Mn(III) from 300 to 600 μM would typically enhance BPA degradation, this expected effect was negated by the concurrent increase in PP from 1800 to 3600 μM. Furthermore, in the 20-fold excess experiments, the lowest initial Mn(III) concentration resulted in the most significant BPA degradation (Figure 1a).

Mn(III) consumption was calculated by subtracting the residual Mn(III) concentrations from their initial values. As the degradation of BPA progressed and its concentration decreased (Figure 1a), there was a corresponding increase in the consumption of dissolved Mn(III) (Figure 1b). By examining the relationship between BPA degradation and Mn(III) reduction in solution, we gained valuable insights into the electron transfer dynamics and reaction stoichiometries. During the initial period of the reaction (Figures 1a and b), specifically when Mn(III) consumption was low, as indicated by the data points in Figure 1c, a clear 1:1 linear relationship in the electron transfer between BPA and Mn(III) was observed. However, in certain setups with lower PP:Mn ratios, including those with a 6-fold PP excess at initial Mn(III) concentrations of 100 and 300

μM, and a 20-fold excess at an initial 100 μM Mn(III). As the reaction proceeded, i.e., at higher Mn(III) consumption (Figure 1c), a slight shift was observed as indicated by the legends trend towards the right side of the 1:1 line. This shift indicated an increased electron gain by Mn(III) compared to the loss from BPA oxidation during the later stages of the reaction. This occurrence could be attributed to the further reaction between Mn(III) and BPA degradation derivatives.

3.2 The Effect of PP on BPA Degradation by Mn Oxides

We examined the effects of PP on BPA degradation mediated by three Mn(III)-bearing Mn oxides: δ-MnO_2, γ-MnOOH, and Mn_3O_4, at pH 7.0. In the absence of PP, δ-MnO_2 showed the highest reactivity towards BPA among the three Mn oxides, degrading 73.5% of the initial concentration over a 4-hour period (Figure 2a). γ-MnOOH exhibited initial activity, removing 4.7% in the first hour, and then plateaued (Figure 2d). In contrast, Mn_3O_4 demonstrated negligible BPA degradation ability (< 1.5%) within the 4-hour incubation period (Figure 2g).

Overall, the addition of PP generally enhanced the degradation capacity of BPA by all three Mn oxides by the end of the incubation period. Initially, within the first 20 minutes of the experiments with δ-MnO_2, the removal of BPA was not significantly affected in the presence of PP (Figure 2a). However, higher concentrations of PP led to more BPA degradation after 30 minutes. For γ-MnOOH, increasing PP from 0 to 300 μM facilitated BPA degradation, but a further increase to 1000 μM did not proportionally enhance this degradation (Figure 2d). Intriguingly, a further increase from 1000 to 2000 μM hindered rather than enhanced the reaction. In the case of Mn_3O_4, increased concentrations of PP led to more rapid BPA removal, particularly notable in the first 5 minutes of the reaction (Figure 2g). As the process progressed, BPA degradation consistently followed a linear pattern, where higher concentrations of PP were associated with higher degradation rates. The influence of PP on the degradation of BPA by these three Mn oxides varied significantly, indicating that the underlying reactions were also different.

3.3 The Effect of PP on the Generation of Mn(III) Species during the Degradation Process

In experiments without PP, intermediate Mn(III) was detected in low concentrations for δ-MnO_2 and Mn_3O_4, but not for γ-MnOOH (Figures 2c, f, and i). Generally, a notable increase in Mn(III) levels for all three Mn oxides was observed with rising PP concentrations, a trend observable over the course of the experiments. In the case of Mn_3O_4, Mn(III) concentration reached a plateau at 90 minutes for lower PP concentrations (200

and 500 μM) but it continued to rise at the highest PP concentration (1000 μM) throughout the 4-hour experiments.

Minor dissolution of Mn oxides was also recorded during the BPA degradation process in the absence of PP (Figures 2b, e, and h). Interestingly, the addition of PP was found to synergistically enhance the dissolution of Mn oxides. This implied that the dissolution rates of Mn oxides, in the simultaneous presence of PP and BPA, exceeded the combined rates when each was present separately (Figures 2b, e, h and S3). This phenomenon, often observed when a reductant and a high-affinity ligand are present concurrently [30, 31], suggested an interaction among PP, Mn oxides, and BPA. The increasing trend of total dissolved Mn concentration in the presence of PP correlated well with the rise in Mn(III) species, indicating that PP addition led to an increase in both Mn(III) and total dissolved Mn (Figure 2).

3.4 Characterization of the Solid Phase

We further conducted X-ray photoelectron spectroscopy (XPS) tests to investigate the average oxidation state (AOS) of surface Mn oxides at the end of the reactions. For δ-MnO_2, the AOS of the original mineral was 3.68 (Figure S5 and Table S1). After the 4-hour reaction, the AOS of samples with 200 μM PP was 3.12, which is slightly lower than the AOS of 3.23 observed in samples without PP (Figure 5a and b). This difference is likely due to the higher degradation of BPA in the presence of 200 μM PP (Figure 1a). However, as the PP concentration further increased to 500 and 1000 μM, the AOS also increased to 3.36 and 3.35 (Figure 5c and d). For γ-MnOOH, which is a monovalent mineral consisting only of Mn(III), the pristine oxide had an AOS of 3.0 (Figure S5 and Table S2). At the end of the reaction, the AOS decreased to 2.72 in the absence of PP. With increasing PP concentrations, the AOS slightly increased to 2.74, 2.81 and 2.82, respectively. For Mn_3O_4, a mixed-valent Mn oxide with the chemical formula $Mn^{II}Mn_2^{III}O_4$, XPS fitting provided an AOS of 2.68 (Figure S5 and Table S3), close to the theoretical level of 2.67. In the absence of PP, the AOS decreased to 2.47 (Figure 5i). While in the presence of PP, though more BPA was degraded (Figure 1c), the AOS increased to 2.53, 2.62, and 2.63 at respective PP concentrations (Figure 5j, k and l).

4. Discussion

4.1 The Effect of PP on BPA Degradation by Different Mn(III) Species

4.1.1 BPA Degradation by Mn(III)-PP Complexes

Dissolved Mn(III) complexes in the presence of a low concentration of PP degraded BPA effectively (Figure 1a), corroborating findings from earlier studies [5, 21]. Moreover, at a lower ratio of PP to Mn (6:1), an increase in Mn(III) concentration from 100 to 300 μM increased the degradation of BPA. However, as the concentration of Mn(III) continued to rise, the degradation rate did not follow a proportional increase, which could be attributed to the relatively low concentration of BPA compared to Mn(III). Additionally, 4-hydroxycumyl alcohol (HCA), which was a primary product of BPA degradation by oxidized Mn species, also consumed part of the Mn(III), although at a rate five times slower than BPA [32]. In previous studies, Mn(III)-PP complexes were commonly added to achieve desired Mn(III) concentrations for initiating BPA degradation [5, 21]. Consistent with our experimental results, in these studies, further increasing Mn(III) did not proportionally enhance the degradation process. This phenomenon may be attributed to the excessively high PP concentrations introduced alongside the increase in Mn(III).

Our findings demonstrate that an elevated concentration of PP markedly suppresses the degradation of BPA, as evidenced by our experimental data. Specifically, at equal concentrations of Mn(III), the rate of BPA degradation was lower in samples with higher concentrations of PP (Figure 1a). Moreover, within the group with a PP:Mn(III) ratio of 20:1, the lowest Mn(III) concentration resulted in the highest rate of BPA degradation. This pattern suggested that an excess of PP dominated the interaction between BPA and Mn(III), hindering the degradation process. A parallel trend was observed in the reaction of Mn(III)-PP complexes with PbO_2 in the presence of excessive PP, and as the concentration of PP increased, the reaction rate decreased and ultimately ceased at a PP excess of 500 times [24]. Additionally, a lag phase was noted at the highest PP concentration at a PP:Mn ratio of 20:1. This phenomenon is likely due to higher PP concentrations obstructing the ligand exchange necessary for electron transfer between Mn(III) complexes and BPA, which was a crucial step in the degradation process [33, 34].

Our analysis of electron transfer between Mn(III) and BPA revealed a 1:1 ratio in the initial reaction period, suggesting that the reaction between BPA and Mn(III)-PP was a single-electron transfer process. However, at the end of the experiment, this ratio deviated slightly from the 1:1 ratio in systems with lower PP

concentrations (below 3600 μM), probably due to interactions between Mn(III) and BPA degradation derivatives [21, 32]. It is worth noting that in the system with high concentrations of PP, the consumption of BPA and Mn(III) maintained a close 1:1 ratio throughout the entire experimental period. This result further indicated that high PP concentrations could not only suppress the reaction between Mn(III) and BPA, but also inhibit further reactions between Mn(III) and BPA degradation derivatives.

4.1.2 Reaction Mechanisms of BPA Degradation by Mn oxides

For δ-MnO_2, rapid degradation of BPA was observed within 240 minutes in the absence of PP (Figure 2a). Previous studies have shown that both surface Mn(IV) (>Mn(IV)) and Mn(III) sites (>Mn(III)) in Mn oxides are reactive towards BPA, facilitating oxidation through a single-electron-transfer step (Eqs. 1 and 2). This reaction generated a BPA radical and resulted in the formation of either Mn(III) or Mn(II) [21, 35, 36]:

$$>Mn(IV) + BPA = Mn(III) + BPA^{\cdot+} \quad (1)$$

$$>Mn(III) + BPA = Mn(II) + BPA^{\cdot+} \quad (2)$$

In the oxidative degradation of BPA by MnO_2, the percentage of Mn(III) played a more important role than the contribution of other properties, including interfacial conductivity, surface area, and surface oxygen species [20], and MnO_2 lacking surface Mn(III) degraded BPA much more slowly [21]. The presence of PP notably enhanced BPA degradation by MnO_2, with the reaction rate increasing as the PP concentration increased (Figure 2a). We proposed that the mechanism behind the above results was that the ligand affected Mn(III) species by binding with the active Mn(III) sites on the mineral surface as well as complexing with intermediate Mn(III) species generated from Eq. 1. In the absence of PP, $Mn(III)_{(aq)}$ would disproportionate to form MnO_2 and dissolved Mn(II), with Mn(II) potentially readsorbing to minerals surfaces, which would decelerate the reaction between δ-MnO_2 and BPA [37-39]. However, in the presence of PP, intermediate $Mn(III)_{(aq)}$ and Mn(II) could be stabilized to form Mn(III)-PP complexes (Eq. 3 and Figure 2c) and Mn(II)-PP, thus increasing the concentration of Mn(III) complexes and mitigating Mn(II) readsorption. This could be further evidenced by the higher AOS of surface Mn oxides in the presence of higher PP concentrations, due to the desorption of Mn(II) induced by PP (Figure 5 and Table S1). Additionally, the co-existence of PP and BPA enhanced the dissolution of Mn oxides, likely inducing the formation of more reactive Mn(III) species (Figure 2c), including both newly exposed reactive surface sites and the intermediate reactive dissolved

Mn(III)-PP complexes. Meanwhile, PP detached Mn(III) from surface sites (Eq. 4), forming dissolved Mn(III) complexes that would further enhance BPA degradation (Eq. 5).

$$Mn(III)_{(aq)} + PP = Mn(III)\text{-}PP \quad (3)$$

$$>Mn(III) + PP = Mn(III)\text{-}PP \quad (4)$$

$$Mn(III)\text{-}PP + BPA = Mn(II) + BPA^{\cdot+} + PP \quad (5)$$

Another noteworthy phenomenon was the synergistic dissolution effect previously mentioned, which could be partially attributed to ligand-promoted mineral dissolution. This process was well-documented in systems that involve multiple ligands with Mn and Fe oxides. Saal and Duckworth reported that multiple ligands enhanced the dissolution of Mn oxides by forming Mn(III)-ligand complexes as intermediates or by facilitating dissolved Mn(II) formation through intermolecular electron transfer [40]. Comparable mechanisms have been proposed for goethite dissolution, involving structural labilization, ligand-mediated Fe(II) detachment, and delayed reoxidation [30].

In our case, PP, a redox-inert ligand, likely interacted with Mn(III) sites without affecting Mn(IV) sites. The single-electron transfer reaction between Mn(IV) and BPA likely generated Mn(III) species, which would remain within the mineral lattice or undergo disproportionation in the absence of PP [22]. However, in the presence of PP, Mn(III) was complexed into the aqueous phase, thereby facilitating the dissolution of Mn oxides, as evidenced by the decreased Mn(III) content on the mineral surface (Figure 5a, b, c, d and Table S1). Another mechanism possibly contributing to this enhanced dissolution involved the formation of the Mn(II)-PP complexes, which alleviated the promoting effect of Mn(II) on the recrystallization process of Mn oxides as well as its tendency to incorporate into the Mn oxides [41]. Moreover, these mechanisms could be evidenced by the fact that the AOS of δ-MnO_2 increased in the presence of PP, due to decreased Mn(II) and Mn(III) content even more BPA was degraded than in the absence of PP (Figure 5a, b, c, d and Table S1).

For γ-MnOOH, it attracted our attention as a representative of trivalent Mn oxides because of the significant role of Mn(III) species and its intricate interplay with PP and BPA. We tested the oxidative reactivity of γ-MnOOH towards BPA and found that it exhibited limited reactivity in the absence of PP (Figure 2d). The addition of PP significantly enhanced BPA degradation and higher PP concentrations appeared to facilitate the dissolution of γ-MnOOH, leading to the formation of Mn(III)-PP complexes, as indicated by the rising levels of Mn(III) and Mn_{dis} (Figures 2e and f). However, under conditions with much higher PP

concentration, more surface and dissolved Mn(III) was complexed by PP, reducing the probability of BPA to competitively complex with Mn(III). This was the reason why the degradation rate of BPA did not proportionally increase significantly under high-concentration PP conditions as shown in Figure 2d and also observed in the separate Mn(III)-PP experiments (Figure 1b). This proposed reaction mechanism was further supported by the observation that, in the absence of PP, γ-MnOOH showed the lowest AOS due to the accumulation of surface Mn(II) during the BPA degradation by γ-MnOOH (Figure 5e, f, g, and h). However, as PP concentration increased, despite enhanced degradation that would typically lower the AOS, the AOS of γ-MnOOH increased. This suggested that PP mitigated the readsorption of Mn(II) onto the mineral surface and promoted the detachment of reduced Mn(II), similar to the effect observed with δ-MnO_2.

For Mn_3O_4, we observed a linear increase in BPA degradation correlating with the rising concentration of PP (Figure 2g). Notably, Mn_3O_4 showed no oxidative capacity towards BPA in the absence of PP, leading us to deduce that BPA degradation predominantly occurs through Mn(III)-PP complexes formed from ligand-assisted mineral dissolution:

$$Mn^{II}Mn_2^{III}O_4 + 2\ PP = 2\ Mn(III)\text{-}PP + Mn(II) \quad (6)$$

In this scenario, PP initially induced the dissolution of Mn_3O_4, resulting in the formation of Mn(III) complexes that actively participated in BPA degradation. This was evidenced by the plateaued Mn(III) and the continued increase of total dissolved Mn (Mn_{dis}) concentrations, suggesting that PP facilitates the dissolution of Mn_3O_4 to produce Mn(III) at a rate slightly higher than the consumed rate by BPA degradation. The initial accumulation of dissolved Mn(III) suggested that labile Mn(III) on the surface of Mn_3O_4, which might have undergone proton-promoted dissolution to form Mn(II) and γ-MnOOH in the absence of PP [42], formed Mn(III)-PP complexes (Figure 2i) under this situation, facilitating swift BPA degradation within the first 10 minutes, a timescale consistent with the expected rate of proton-promoted Mn_3O_4 dissolution [43], further substantiating our hypothesis. Additionally, similar to γ-MnOOH, an increase in AOS of Mn_3O_4 was also noted, which could be attributed to the enhanced Mn(II) detachment in the presence of PP, as well as the mitigated readsorption of reduced Mn(II).

4.2 Critical Role of Mn(III) Species in BPA Degradation

Both dissolved Mn(III) and solid Mn(III) in Mn oxides could effectively degrade BPA, and the presence of ligands significantly affected the dissolved Mn(III) produced from the dissolution of solid minerals. PP, a

typical ligand, coordinates with Mn(III) to form Mn(III)-PP complexes, in which the Mn(III) center is chelated by four terminal phosphate oxygen atoms. This coordination geometry aligns with the Jahn-Teller distortion of the $Mn(III)O_6$ coordination environment, characterized by the elongation of two axial Mn–O bonds and the contraction of four equatorial ones [44]. In our experiments, we observed that Mn(III) species likely oxidized BPA through a single-electron transfer process (Figure 1c) as it did towards other organic pollutants [27, 33]. Mn(III) formed an inner-sphere complex with BPA via its empty σ orbital, facilitating electron transfer [20, 45]. In contrast, the oxidation of BPA by Mn(IV) appeared to proceed via an outer-sphere electron transfer process, necessitating a change in the spin state due to the higher energy requirement for forming an inner-sphere complex [20, 46]. It is well-known that aqueous Mn(III) ions tend to disproportionate, forming MnO_2 precipitates and dissolved Mn(II) [11, 17]. This instability underscored the importance of ligand stabilization in maintaining Mn(III) in a form that can effectively degrade organic pollutants [26, 47]. For instance, the addition of picolinic acid (PICA) could mediate Mn(II) activation by peracetic acid, accelerating micropollutant degradation through the formation of metastable Mn(III)-PICA complexes [48]. Similarly, it was reported that Mn(III)-oxalate complexes enhanced the degradation of tetracycline, though this effectiveness was reduced at higher concentrations of the ligand due to the intermolecular electron transfer from oxalate to Mn(III), resulting in the formation of unreactive Mn(II) [37]. This phenomenon was also observed with Mn(III)-oxalate and Mn(III)-PP complexes in methylmercury degradation [6]. The observed decrease in BPA degradation by γ-MnOOH with a higher concentration of PP further validated our hypothesis, as Mn(III) species overly coordinated with ligands have been proved to be less reactive and accessible compared to those in low ligand-to-metal ratios [6, 17, 49].

The high reactivity of Mn(III) in Mn oxides has been well documented, and the variation in Mn(III) reactivity and crystal lattice structure across those three Mn oxides was also a significant factor contributing to the difference in their oxidation behavior of BPA. This reactivity can be attributed to the d^4 electron configuration of Mn(III) in the $t_{2g}^3 e_g^1$ state, which leads to an elongated Mn-O bond due to Jahn-Teller distortion [46, 50]. This bond, significantly weaker than the bond formed with Mn(IV), can cause lattice distortions that facilitate easier electron donation in reactions [46, 50]. δ-MnO_2 exhibited markedly higher reactivity toward BPA compared to γ-MnOOH and Mn_3O_4 in the absence of PP, despite the latter two having a higher Mn(III) content. This discrepancy is possibly attributed to their distinct crystallographic structures

[51]. It had been reported that δ-MnO_2, compared to Mn_3O_4 and Mn_2O_3, have layered structures and large surface areas that facilitate solutes to active sites and promote electron transfer between different Mn valence states (III/IV), which might be a crucial step in the degradation of BPA [52, 53]. From these results, we inferred that in the case of δ-MnO_2, where Mn(IV) sites exist, electron transfer may happen concurrently within the lattice structure between Mn(III) and Mn(IV) as well as between surficial Mn(III, IV) sites and BPA. On the contrary, in the cases of γ-MnOOH and Mn_3O_4, the reaction dynamics appear to be predominantly confined to surface interactions, possibly restricted by their comparatively smaller surface areas. This limitation likely contributed to the observed slower rates of BPA degradation by γ-MnOOH and Mn_3O_4 (Figure 2). The low reactivity of γ-MnOOH towards BPA could be attributed to the limited number of reactive surface sites in the 1×1 tunnels of γ-MnOOH, which failed to accommodate other chemical species [54]. In contrast to its higher oxidative reactivity for Cr(III) and As(III) at acidic pH [55-57], Mn_3O_4 demonstrated negligible dissolution at pH 7.0 in our experiments in the absence of PP (Figure S4), thereby rendering reactive Mn(III) sites unavailability towards the oxidation of BPA. Overall, these results not only emphasize the importance of intermediate Mn(III) species from the mineral dissolution in BPA degradation but also illustrate the distinct behavior of Mn(III) in varied Mn oxides due to their different crystallographic locations, affecting their ability to engage in electron transfer processes.

4.3 Kinetic Modeling

To ascertain the specific rate constants and validate our hypothesized reaction pathways for BPA degradation by Mn oxides, we utilized kinetic modeling to fit our experimental data (Figure 2). This approach was grounded in several key assumptions: (1) each reactant exhibited first-order kinetic behavior; (2) the reactions conformed to the stoichiometry outlined in Eqs. 1-6, and (3) while the PP concentration was not directly included in the differential equations, its effect was implied through the reaction rate constants obtained from fitting the kinetic data. The rate constant k_1' denoted the reaction rate constant of BPA oxidation by Mn(IV) in δ-MnO_2 (Eq. 1), and k_1 denoted the rate constant of the reaction between BPA and Mn(III) in Mn oxides (Eq. 2). k_3 denoted the rate constant of reaction between BPA and dissolved Mn(III)-PP (Eq. 5). A constant k_4 was also introduced to reflect the inhibitory effect of Mn(II) generated on the reaction rates [58]. To note that, this assumption did not imply a direct reaction between Mn(II) and >Mn(III), but rather encompasses the combined inhibitory effects resulting from Mn(II) readsorption and competition

for reactive sites [34, 39]. To enhance comprehension of the proposed reaction mechanisms, the rate constants k_1', k_1, k_3, k_4 are matched with the pathways labeled as (a), (b), (c), and (d) in Figure 4, respectively.

For δ-MnO_2:

$$\frac{\mathrm{d[BPA]}}{\mathrm{d}t} = -k_1[\mathrm{BPA}][>\mathrm{Mn(III)}] - k_1'[\mathrm{BPA}][>\mathrm{Mn(IV)}] - k_3[\mathrm{BPA}][\mathrm{Mn(III)}] \quad (7)$$

$$\frac{\mathrm{d[Mn(III)]}}{\mathrm{d}t} = k_2[>\mathrm{Mn(III)}] - k_3[\mathrm{BPA}][\mathrm{Mn(III)}] \quad (8)$$

$$\frac{\mathrm{d[Mn_{tot}]}}{\mathrm{d}t} = k_1[\mathrm{BPA}][>\mathrm{Mn(III)}] + k_2[>\mathrm{Mn(III)}] \quad (9)$$

$$\frac{\mathrm{d[>Mn(III)]}}{\mathrm{d}t} = -k_1[\mathrm{BPA}][>\mathrm{Mn(III)}] - k_2[>\mathrm{Mn(III)}] - k_4[>\mathrm{Mn(III)}][\mathrm{Mn(II)}] \quad (10)$$

$$\frac{\mathrm{d[>Mn(IV)]}}{\mathrm{d}t} = -k_1'[\mathrm{BPA}][>\mathrm{Mn(IV)}] - k_4[>\mathrm{Mn(IV)}][\mathrm{Mn(II)}] \quad (11)$$

Notably, in the absence of PP, we observed that the total dissolved Mn (Mn_{dis}) measured was under 10 moles (Figure 2b), whereas BPA degradation exceeded 73.5 moles (Figure 2a). Upon closer examination (Text S5), the significant electron transfer imbalance between reduced Mn(IV) and oxidized BPA led us to deduce that Mn(III), rather than existing as dissolved Mn(III) in the aqueous phase, was more likely incorporated into the lattice structure, a finding supported by Balgooyen et al. [22]. To assess the reactivity of these Mn(III) entities, we hypothesized that they would exhibit similar reactivity to pre-existing Mn(III) sites. This hypothesis, however, did not align with our experimental outcomes and was consequently dismissed. Summarizing, our refined model suggests that the interaction between BPA and Mn(IV) primarily results in the generation of non-reactive Mn(III) sites.

For γ-MnOOH:

$$\frac{\mathrm{d[BPA]}}{\mathrm{d}t} = -k_1[\mathrm{BPA}][\mathrm{MnOOH}] - k_3[\mathrm{BPA}][\mathrm{Mn(III)}] \quad (12)$$

$$\frac{\mathrm{d[Mn(III)]}}{\mathrm{d}t} = k_2[\mathrm{MnOOH}] - k_3[\mathrm{BPA}][\mathrm{Mn(III)}] \quad (13)$$

$$\frac{\mathrm{d[Mn_{tot}]}}{\mathrm{d}t} = k_1[\mathrm{MnOOH}][\mathrm{BPA}] + k_2[\mathrm{MnOOH}] \quad (14)$$

$$\frac{\mathrm{d[MnOOH]}}{\mathrm{d}t} = -k_1[\mathrm{BPA}][\mathrm{MnOOH}] - k_2[>\mathrm{Mn(III)}] - k_4[\mathrm{MnOOH}][\mathrm{Mn(II)}] \quad (15)$$

For Mn_3O_4, a $Mn^{III}Mn^{II}_{0.5}$ unit was applied to avoid complicated stoichiometries:

$$\frac{d[BPA]}{dt} = -k_1[BPA][Mn^{III}Mn^{II}_{0.5}] - k_3[BPA][Mn(III)] \quad (16)$$

$$\frac{d[Mn(III)]}{dt} = k_2[Mn^{III}Mn^{II}_{0.5}] - k_3[BPA][Mn(III)] \quad (17)$$

$$\frac{d[Mn_{tot}]}{dt} = \frac{3}{2}k_1[Mn^{III}Mn^{II}_{0.5}][BPA] + \frac{3}{2}k_2[Mn^{III}Mn^{II}_{0.5}] \quad (18)$$

$$\frac{d[Mn^{III}Mn^{II}_{0.5}]}{dt} = -k_1[BPA][Mn^{III}Mn^{II}_{0.5}] - k_2[Mn^{III}Mn^{II}_{0.5}] - k_4[Mn^{III}Mn^{II}_{0.5}][Mn(II)] \quad (19)$$

For all the above models, the concentration of Mn(II) was calculated by subtracting Mn(III) from the total dissolved Mn (Mn_{dis}). Direct calculations of electron transfer for Mn oxides and BPA were not presented, given that the excellent alignment of model results with the experimental data implicitly validated electron transfer balance based on the proposed reaction pathways.

Upon fitting our kinetic data to these numerical models, we determined the rate constants $k_1(k_1')$, k_2, k_3, k_4, which are detailed in Table 1. Our model effectively quantified the influence of the PP:Mn ratio on BPA degradation by Mn oxides. The alignment of our model results with all experimental data, including the behavior of BPA and total dissolved Mn over time, was remarkably accurate (Figure 2). Our analysis revealed that the rate constant $k_1(k_1')$ for BPA degradation by Mn oxides showed minimal variance, indicating a weak dependence on PP:Mn ratio. In contrast, the rate constant k_2 increased with an elevated PP:Mn ratio. Conversely, the rate constant k_3 decreased with increasing PP concentrations across all Mn oxides studied. Notably, as PP concentration increased, the binding capacity of Mn(II) to mineral surfaces decreased, leading to a diminished reaction rate. This effect, marked by a reduction in k_4, was prominent in γ-MnOOH and M_3O_4. For δ-MnO_2, this trend was less pronounced due to the potential formation of Mn(III) through comproportionation of Mn(II) with surface Mn(IV) sites [38]. Despite the lower affinity of PP for Mn(II) compared to Mn(III), its ability to form complexes still alleviated Mn(II) adsorption onto mineral surfaces, influencing the reaction rates [44, 59], as reflected by the increased AOS in Mn oxides in the presence of PP (Figure 5). Further enhancing our understanding, the kinetic model enabled us to quantify the contributions of different reaction pathways to BPA degradation at the end of the batch experiments (Figure 3). The contribution to BPA degradation was divided into two parts, either by Mn oxides or by aqueous Mn(III) species and is detailed as follows. For δ-MnO_2, the degradation of BPA primarily occurred through the oxide. However,

as the concentration of PP increased, the role of Mn(III) intermediates in the degradation process became more significant, increasing from 6.2% to 38.6% as PP concentration increased from 200 to 1000 μM (Figure 3a). In the case of γ-MnOOH, the oxide itself was predominantly responsible for BPA degradation, accounting for 96.5% and 87.8% of total degraded BPA in the presence of 300 and 1000 μM PP, respectively (Figure 3b). Nonetheless, an increase in PP concentration from 1000 to 2000 μM appeared to slightly reduce the contribution of the oxide to 86.1% (Figure 3b). This reduction may be attributed to competitive binding between BPA and PP, as evidenced by a corresponding increase in the degradation contribution from Mn(III) intermediates. For Mn_3O_4, the oxide continued to be the primary pathway for BPA degradation, which was notably enhanced in the presence of PP, increasing from 53.4% to 73.8% when PP concentration increased from 200 to 1000 μM (Figure 3c). This enhancement is likely due to the labilization of the mineral structure and a reduction in Mn(II) readsorption, which exposes more reactive sites for degradation. Combining these results, we suggest that despite PP inducing homogeneous degradation of BPA by aqueous Mn(III) species, heterogeneous degradation by Mn oxides still remains the predominant reaction pathway. The kinetic insights derived align closely with the hypothesized reaction pathways, substantiating the diverse reactivity of Mn(III) species and unveiling the multifaceted effect of PP on BPA degradation by Mn oxides.

5. Conclusions

In this study, we identified the critical Mn(III)-mediated reaction mechanisms for BPA degradation, as depicted in Figure 4: (a) BPA initially forms a surface complex with Mn(IV) on the Mn oxides, initiating a single-electron transfer [60]. This reaction leads to the detachment of intermediate Mn(III) ions from the mineral lattice, which then stabilize in solution by forming complexes with PP; (b) BPA also complexes with surface Mn(III), followed by an electron transfer which results in the liberation of Mn(II) into the solution. Meanwhile, PP can also complex with surface Mn(III), resulting in the formation of soluble Mn(III)-PP complexes; (c) BPA undergoes ligand exchange with Mn(III) complexes, facilitating a single-electron transfer and subsequent release of Mn(II) and PP into the solution; (d) The likelihood of BPA forming complexes with surface Mn(III) is diminished by the adsorption of Mn(II) onto mineral surfaces, a process which PP counteracts by forming Mn(II)-PP complexes. Additionally, the interaction of Mn(II) with surface Mn(IV) sites leads to the formation of surface Mn(III), which is then detached from the mineral surface and stabilized

in solution by forming dissolved Mn(III)-PP complexes. By studying the role of PP in detail, we answered why increasing initial Mn(III) concentrations did not proportionally increase the degradation rate [5], and provided plausible explanations for why PP enhanced the degradation of BPA by MnO_2 of different structures, but to different extents [20]. These findings enhance our understanding of the Mn oxide-mediated degradation of BPA, offering a more precise quantitative assessment of the role of dissolved Mn(III) intermediates in the process. The interaction of these mechanisms with natural soil components like PP highlights the complex dynamics of organic pollutants in natural environments, pointing to broader implications for environmental health and safety.

Acknowledgments

This work was funded by the National Natural Science Foundation of China (42307320, 41977266, and 42377402), the National Key R&D Program of China (2023YFC3708802) and the China Postdoctoral Science Foundation (2024M761283, and GZC20240644). Effort by Dr. Peng Yang was supported by the U.S. Department of Energy, Office of Science, Office of Basic Energy Sciences, Chemical Sciences, Geosciences, and Biosciences Division.

References:

[1] C.K. Remucal, M. Ginder-Vogel, A critical review of the reactivity of manganese oxides with organic contaminants, Environmental Science: Processes & Impacts, 16 (2014) 1247-1266.
[2] H. Li, F. Santos, K. Butler, E. Herndon, A Critical Review on the Multiple Roles of Manganese in Stabilizing and Destabilizing Soil Organic Matter, Environmental Science & Technology, 55 (2021) 12136-12152.
[3] R.E. Trouwborst, B.G. Clement, B.M. Tebo, B.T. Glazer, G.W. Luther, Soluble Mn(III) in Suboxic Zones, Science, 313 (2006) 1955-1957.
[4] K.S. Johnson, Manganese Redox Chemistry Revisited, Science, 313 (2006) 1896-1897.
[5] Y. Sun, J. Im, N. Shobnam, S.K. Fanourakis, L. He, L.M. Anovitz, P.R. Erickson, H. Sun, J. Zhuang, F.E. Löffler, Degradation of Adsorbed Bisphenol A by Soluble Mn(III), Environmental Science & Technology, 55 (2021) 13014-13023.
[6] S. Zhang, B. Li, Y. Chen, M. Zhu, J.A. Pedersen, B. Gu, Z. Wang, H. Li, J. Liu, X.-Q. Zhou, Y.-Y. Hao, H. Jiang, F. Liu, Y.-R. Liu, H. Yin, Methylmercury Degradation by Trivalent Manganese, Environmental Science & Technology, (2023).
[7] S. Wang, J. Chen, Y. Sun, B. Sun, J. Qiao, X. Guan, Roles of MnO_2 Colloids and Mn(III) during the Oxidation of Organic Contaminants by Permanganate, Environmental Science & Technology, 57 (2023) 997-1005.
[8] W. Zhao, H. Cui, F. Liu, W. Tan, X. Feng, Relationship between Pb^{2+} adsorption and average Mn oxidation state in synthetic birnessites, Clays and Clay Minerals, 57 (2009) 513-520.
[9] M. Zhu, M. Ginder-Vogel, S.J. Parikh, X.-H. Feng, D.L. Sparks, Cation Effects on the Layer Structure of Biogenic Mn-Oxides, Environmental Science & Technology, 44 (2010) 4465-4471.
[10] A.T. Stone, Reductive Dissolution of Manganese(III/IV) Oxides by Substituted Phenols, Environmental Science & Technology, 21 (1987) 979-988.
[11] J.E. Kostka, G.W. Luther, K.H. Nealson, Chemical and biological reduction of Mn(III)-pyrophosphate complexes: Potential importance of dissolved Mn(III) as an environmental oxidant, Geochimica et Cosmochimica Acta, 59 (1995) 885-894.

[12] M.E. Jones, P.S. Nico, S. Ying, T. Regier, J. Thieme, M. Keiluweit, Manganese-Driven Carbon Oxidation at Oxic-Anoxic Interfaces, Environmental Science & Technology, 52 (2018) 12349-12357.
[13] M.E. Jones, R.E. LaCroix, J. Zeigler, S.C. Ying, P.S. Nico, M. Keiluweit, Enzymes, Manganese, or Iron? Drivers of Oxidative Organic Matter Decomposition in Soils, Environmental Science & Technology, 54 (2020) 14114-14123.
[14] G.W. Luther III, A.S. Madison, A. Mucci, B. Sundby, V.E. Oldham, A kinetic approach to assess the strengths of ligands bound to soluble Mn (III), Marine Chemistry, 173 (2015) 93-99.
[15] V.E. Oldham, A. Mucci, B.M. Tebo, G.W. Luther, Soluble Mn(III)–L complexes are abundant in oxygenated waters and stabilized by humic ligands, Geochimica et Cosmochimica Acta, 199 (2017) 238-246.
[16] T.M. McBeath, R.J. Smernik, E. Lombi, M.J. McLaughlin, Hydrolysis of Pyrophosphate in a Highly Calcareous Soil, Soil Science Society of America Journal, 70 (2006) 856-862.
[17] A. Qian, W. Zhang, C. Shi, C. Pan, D.E. Giammar, S.H. Yuan, H.L. Zhang, Z.M. Wang, Geochemical Stability of Dissolved Mn(III) in the Presence of Pyrophosphate as a Model Ligand: Complexation and Disproportionation, Environmental Science & Technology, 53 (2019) 5768-5777.
[18] P.S. Nico, R.J. Zasoski, Importance of Mn(III) Availability on the Rate of Cr(III) Oxidation on δ-MnO_2, Environmental Science & Technology, 34 (2000) 3363-3367.
[19] P.S. Nico, R.J. Zasoski, Mn (III) center availability as a rate controlling factor in the oxidation of phenol and sulfide on δ-MnO_2, Environmental Science & Technology, 35 (2001) 3338-3343.
[20] J. Huang, S. Zhong, Y. Dai, C.-C. Liu, H. Zhang, Effect of MnO_2 Phase Structure on the Oxidative Reactivity toward Bisphenol A Degradation, Environmental Science & Technology, 52 (2018) 11309-11318.
[21] Y. Sun, C. Wang, A.L. May, G. Chen, Y. Yin, Y. Xie, A.M. Lato, J. Im, F.E. Löffler, Mn(III)-mediated bisphenol a degradation: Mechanisms and products, Water Research, 235 (2023) 119787.
[22] S. Balgooyen, P.J. Alaimo, C.K. Remucal, M. Ginder-Vogel, Structural transformation of MnO_2 during the oxidation of bisphenol A, Environmental Science & Technology, 51 (2017) 6053-6062.
[23] T. Zhang, X. Zhang, X. Yan, J. Ng, Y. Wang, D.D. Sun, Removal of bisphenol A via a hybrid process combining oxidation on β-MnO_2 nanowires with microfiltration, Colloids and Surfaces A: Physicochemical and Engineering Aspects, 392 (2011) 198-204.
[24] X. Wang, Q. Wang, P. Yang, X. Wang, L. Zhang, X. Feng, M. Zhu, Z. Wang, Oxidation of Mn(III) Species by Pb(IV) Oxide as a Surrogate Oxidant in Aquatic Systems, Environmental Science & Technology, 54 (2020) 14124-14133.
[25] X. Yu, J. Xue, H. Yao, Q. Wu, A.K. Venkatesan, R.U. Halden, K. Kannan, Occurrence and estrogenic potency of eight bisphenol analogs in sewage sludge from the U.S. EPA targeted national sewage sludge survey, Journal of Hazardous Materials, 299 (2015) 733-739.
[26] E. Hu, Y. Zhang, S. Wu, J. Wu, L. Liang, F. He, Role of dissolved Mn(III) in transformation of organic contaminants: Non-oxidative versus oxidative mechanisms, Water Research, 111 (2017) 234-243.
[27] W.-R. Chen, C. Liu, S.A. Boyd, B.J. Teppen, H. Li, Reduction of Carbadox Mediated by Reaction of Mn(III) with Oxalic Acid, Environmental Science & Technology, 47 (2013) 1357-1364.
[28] S.M. Webb, G.J. Dick, J.R. Bargar, B.M. Tebo, Evidence for the presence of Mn(III) intermediates in the bacterial oxidation of Mn(II), Proceedings of the National Academy of Sciences, 102 (2005) 5558-5563.
[29] X. Wang, J. Wang, X. Lu, M. Zhou, Q. Wang, Z. Pan, N. Kumar, M. Zhu, Z. Wang, Oxidative dissolution of orpiment and realgar induced by dissolved and solid Mn(III) species, Geochimica et Cosmochimica Acta, 332 (2022) 307-326

[30] Z. Wang, W.D.C. Schenkeveld, S.M. Kraemer, D.E. Giammar, Synergistic Effect of Reductive and Ligand-Promoted Dissolution of Goethite, Environmental Science & Technology, 49 (2015) 7236-7244.
[31] W.D.C. Schenkeveld, Z. Wang, D.E. Giammar, S.M. Kraemer, Synergistic Effects between Biogenic Ligands and a Reductant in Fe Acquisition from Calcareous Soil, Environmental Science & Technology, 50 (2016) 6381-6388.
[32] J. Im, C.W. Prevatte, S.R. Campagna, F.E. Löffler, Identification of 4-Hydroxycumyl Alcohol As the Major MnO_2-Mediated Bisphenol A Transformation Product and Evaluation of Its Environmental Fate, Environmental Science & Technology, 49 (2015) 6214-6221.
[33] E.L. Trainer, M. Ginder-Vogel, C.K. Remucal, Organic structure and solid characteristics determine reactivity of phenolic compounds with synthetic and reclaimed manganese oxides, Environmental Science: Water Research & Technology, 6 (2020) 540-553.

[34] E.L. Trainer, M. Ginder-Vogel, C.K. Remucal, Enhancement and Inhibition of Oxidation in Phenolic Compound Mixtures with Manganese Oxides, ACS ES&T Water, 2 (2022) 2400-2408.
[35] N. Gao, J. Hong, Z. Yu, P. Peng, W. Huang, Transformation of Bisphenol A in the Presence of Manganese Dioxide, Soil Science, 176 (2011).
[36] N. Shaikh, S. Taujale, H. Zhang, K. Artyushkova, A.-M.S. Ali, J.M. Cerrato, Spectroscopic Investigation of Interfacial Interaction of Manganese Oxide with Triclosan, Aniline, and Phenol, Environmental Science & Technology, 50 (2016) 10978-10987.
[37] S. Sun, Y. Wang, L. Zhou, X. Wang, C. Kang, Enhanced degradation mechanism of tetracycline by MnO_2 with the presence of organic acids, Chemosphere, 286 (2022) 131606.
[38] D. Jia, M. Brigante, C. Zhang, G. Mailhot, Impact of Mn^{2+} in bisphenol A degradation by chelating agents-assisted manganese dioxide: Mechanism understanding and efficiency evaluation, Journal of Water Process Engineering, 56 (2023) 104388.
[39] J.T. Swenson, M. Ginder-Vogel, C.K. Remucal, Influence of Divalent Cation Inhibition and Dissolved Organic Matter Enhancement on Phenol Oxidation Kinetics by Manganese Oxides, Environmental Science & Technology, (2024).
[40] L.B. Saal, O.W. Duckworth, Synergistic Dissolution of Manganese Oxides as Promoted by Siderophores and Small Organic Acids, Soil Science Society of America Journal, 74 (2010) 2021-2031.
[41] M.A.G. Hinkle, E.D. Flynn, J.G. Catalano, Structural response of phyllomanganates to wet aging and aqueous Mn(II), Geochimica et Cosmochimica Acta, 192 (2016) 220-234.
[42] J.D. Hem, C.J. Lind, Nonequilibrium models for predicting forms of precipitated manganese oxides, Geochimica et Cosmochimica Acta, 47 (1983) 2037-2046.
[43] J. Peña, O.W. Duckworth, J.R. Bargar, G. Sposito, Dissolution of hausmannite (Mn_3O_4) in the presence of the trihydroxamate siderophore desferrioxamine B, Geochimica et Cosmochimica Acta, 71 (2007) 5661-5671.
[44] J.J. Morgan, M.A. Schlautman, H. Bilinski, Rates of Abiotic Mn^{II} Oxidation by O_2: Influence of Various Multidentate Ligands at High pH, Environmental Science & Technology, 55 (2021) 14426-14435.
[45] L. Ukrainczyk, M.B. McBride, Oxidation of Phenol in Acidic Aqueous Suspensions of Manganese Oxides, Clays and Clay Minerals, 40 (1992) 157-166.
[46] U. Maitra, B.S. Naidu, A. Govindaraj, C.N.R. Rao, Importance of trivalency and the e_g^1 configuration in the photocatalytic oxidation of water by Mn and Co oxides, Proceedings of the National Academy of Sciences, 110 (2013) 11704-11707.
[47] Y. Gao, J. Jiang, Y. Zhou, S.-Y. Pang, C. Jiang, Q. Guo, J.-B. Duan, Does Soluble Mn(III) Oxidant Formed in Situ Account for Enhanced Transformation of Triclosan by Mn(VII) in the Presence of Ligands?, Environmental Science & Technology, 52 (2018) 4785-4793.
[48] J. Kim, J. Wang, D.C. Ashley, V.K. Sharma, C.-H. Huang, Picolinic Acid-Mediated Catalysis of Mn(II) for Peracetic Acid Oxidation Processes: Formation of High-Valent Mn Species, Environmental Science & Technology, (2023).
[49] Z. Wang, W. Xiong, B.M. Tebo, D.E. Giammar, Oxidative UO_2 Dissolution Induced by Soluble Mn(III), Environmental Science & Technology, 48 (2014) 289-298.
[50] T. Kohler, T. Armbruster, E. Libowitzky, Hydrogen bonding and Jahn-Teller distortion in groutite, α-MnOOH, and manganite, γ-MnOOH, and their relations to the manganese dioxides ramsdellite and pyrolusite, Journal of Solid State Chemistry, 133 (1997) 486-500.
[51] Y. Meng, W. Song, H. Huang, Z. Ren, S.-Y. Chen, S.L. Suib, Structure–Property Relationship of Bifunctional MnO_2 Nanostructures: Highly Efficient, Ultra-Stable Electrochemical Water Oxidation and Oxygen Reduction Reaction Catalysts Identified in Alkaline Media, Journal of the American Chemical Society, 136 (2014) 11452-11464.
[52] N. Birkner, S. Nayeri, B. Pashaei, M.M. Najafpour, W.H. Casey, A. Navrotsky, Energetic basis of catalytic activity of layered nanophase calcium manganese oxides for water oxidation, Proceedings of the National Academy of Sciences, 110 (2013) 8801-8806.
[53] H. Peng, I.G. McKendry, R. Ding, A.C. Thenuwara, Q. Kang, S.L. Shumlas, D.R. Strongin, M.J. Zdilla, J.P. Perdew, Redox properties of birnessite from a defect perspective, Proceedings of the National Academy of Sciences, 114 (2017) 9523-9528.
[54] V.B.R. Boppana, S. Yusuf, G.S. Hutchings, F. Jiao, Nanostructured Alkaline-Cation-Containing δ-MnO_2 for Photocatalytic Water Oxidation, Advanced Functional Materials, 23 (2013) 878-884.

[55] D. Jarosch, Crystal structure refinement and reflectance measurements of hausmannite, Mn_3O_4, Mineralogy and Petrology, 37 (1987) 15-23.
[56] Y. Cantu, A. Remes, A. Reyna, D. Martinez, J. Villarreal, H. Ramos, S. Trevino, C. Tamez, A. Martinez, T. Eubanks, J.G. Parsons, Thermodynamics, kinetics, and activation energy studies of the sorption of chromium(III) and chromium(VI) to a Mn_3O_4 nanomaterial, Chemical Engineering Journal, 254 (2014) 374-383.
[57] Y. Luo, W.F. Tan, S.L. Suib, G.H. Qiu, F. Liu, Dissolution and phase transformation processes of hausmannite in acidic aqueous systems under anoxic conditions, Chemical Geology, 487 (2018) 54-62.
[58] K. Lin, Y. Peng, X. Huang, J. Ding, Transformation of bisphenol A by manganese oxide-coated sand, Environmental Science and Pollution Research, 20 (2013) 1461-1467.
[59] H. Bilinski, Precipitation and complex formation in the system $Mn(ClO_4)^{2-}Na_4P_2O_7^{-}$-pH (295 K, I = 0.5 and I $\approx$ 0 mol dm^{-3}), Polyhedron, 2 (1983) 353-358.
[60] K. Lin, W. Liu, J. Gan, Oxidative Removal of Bisphenol A by Manganese Dioxide: Efficacy, Products, and Pathways, Environmental Science & Technology, 43 (2009) 3860-3864.

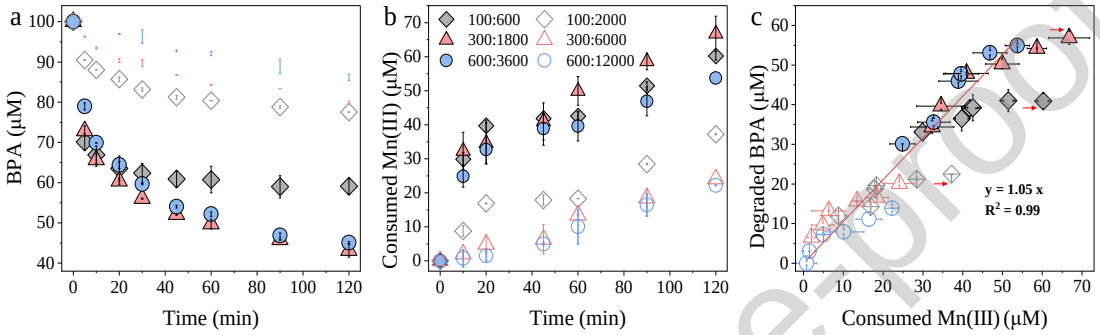

Figure 1. Degradation of 100 μM BPA at pH 7.0 with varied Mn(III):PP ratios over time. (a) Time-course degradation of BPA with Mn(III) at initial concentrations of 100, 300, and 600 μM. Each Mn(III) level is tested with PP at 6-fold and 20-fold molar excess. Legend symbols indicate the Mn(III):PP ratios, with solid symbols representing 6-fold PP excess and open symbols for 20-fold excess, and the legends in panels a and c are the same as in panel b. (b) The amount of consumed Mn(III) calculated from the initial and residual Mn(III) concentrations throughout the BPA degradation process. (c) Correlation between the amount of electron transfer between the oxidant (Mn(III)-PP) and the reductant (BPA) throughout the experiments with different ratios of PP to Mn(III). Three data points (as shown by the red arrow) at the end of the incubation period were excluded for a clearer correlation. At the initial reaction stages, there was a 1:1 mole ratio of electron gain by Mn(III) to electron loss by BPA. Error bars represent the standard deviation from three replicate experiments.

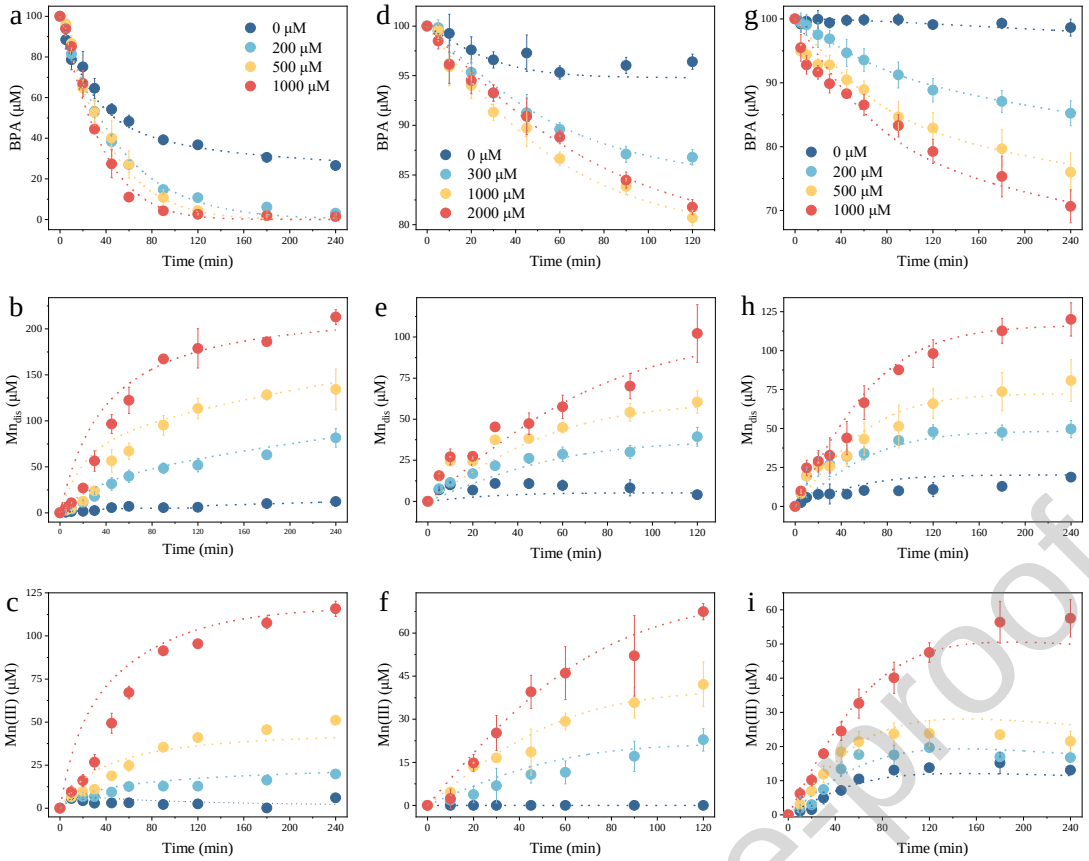

Figure 2. Concentration profiles of BPA, total dissolved Mn (Mn_{dis}) and Mn(III) at pH 7.0 in the process of BPA degradation, using 0.1 g/L of different Mn oxides and varying concentrations of PP over time. (a, b, c) With δ-MnO_2 and initial PP concentrations of 0, 200, 500, and 1000 μM. (d, e, f) With γ-MnOOH and initial PP concentrations of 0, 300, 1000, and 2000 μM. (g, h, i) With Mn_3O_4 and initial PP concentrations of 0, 200, 500, and 1000 μM. Legends for panels b and c, e and f, h and i are the same as those in panels a, d, and g respectively. Experimental data and model simulations are shown as symbols and lines, respectively. Error bars represent the standard deviation from three replicate experiments.

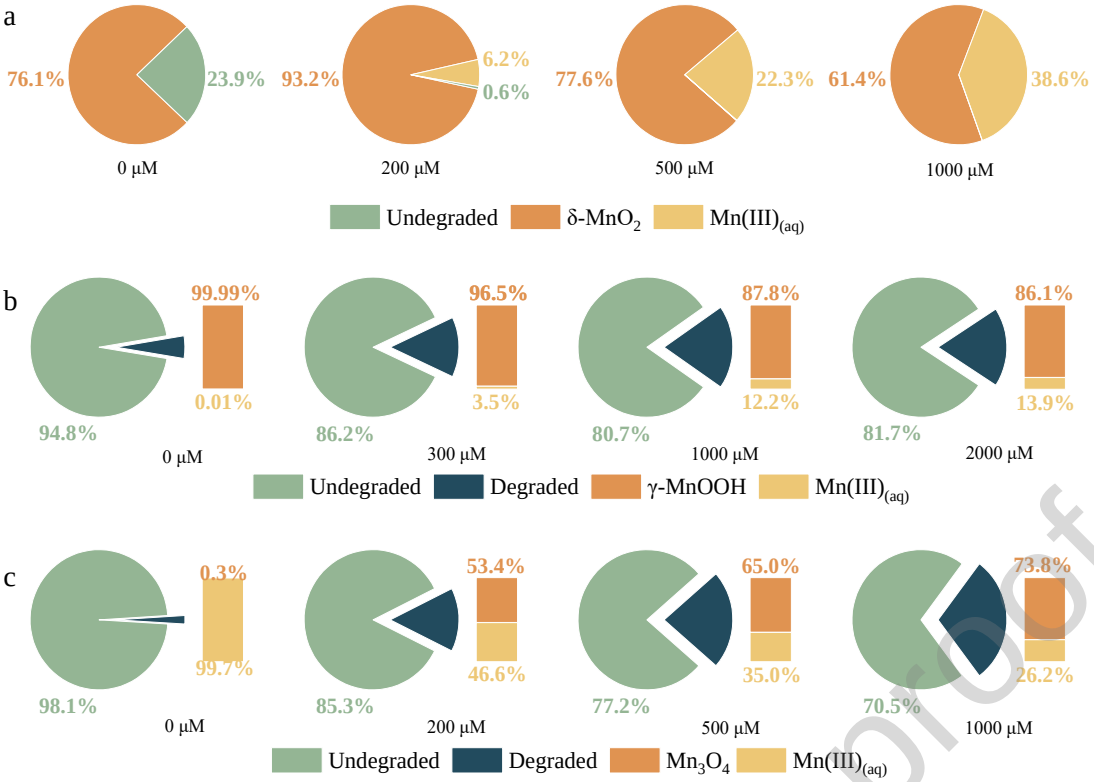

Figure 3. Contribution ratios of BPA degradation pathways, attributed to either Mn oxides or aqueous Mn(III) species. Panels (a) δ-MnO_2, (b) γ-MnOOH, and (c) Mn_3O_4 display results from left to right, indicating increasing concentrations of PP from low (absence of PP) to high. The contribution ratios are calculated based on the kinetic model presented in the main text. Specifically, BPA was near completely degraded in the case of δ-MnO_2, as shown in panel (a). While panels (b) γ-MnOOH and (c) Mn_3O_4 show detailed ratios of BPA degradation by each pathway through bar charts; total degraded percentages are not shown for simplicity.

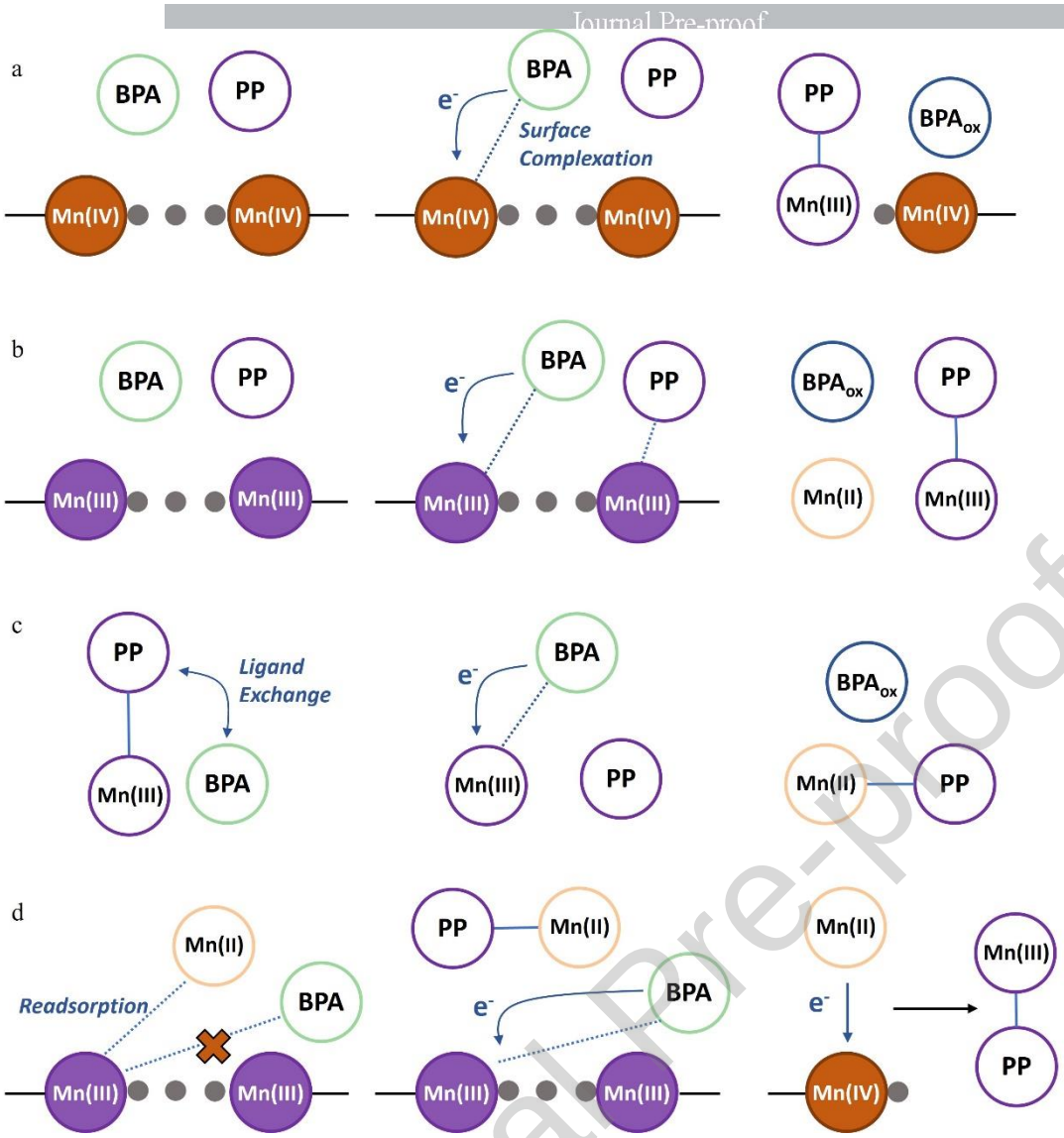

Figure 4. Schematic representation of Mn(III) and PP-mediated pathways for BPA degradation by Mn oxides at circumneutral pH. (a) BPA forms an inner-sphere complex with surface Mn(IV), initiating a single-electron transfer process from BPA to Mn(IV). The resulting Mn(III) ions detach from the mineral lattice and stabilize in solution by complexing with PP. (b) BPA complexes with surface Mn(III), followed by electron transfer, after which Mn(III) binds with PP, forming Mn(III)-PP complexes that, along with Mn(II), release into the solution. (c) BPA undergoes ligand exchange with Mn(III) complexes, facilitating a single-electron transfer and the consequent release of Mn(II) and PP into the solution. (d) In γ-MnOOH and Mn_3O_4, the readsorption of Mn(II) onto mineral surfaces diminishes the likelihood of BPA forming complexes with surface Mn(III), a process that PP mitigates by forming Mn(II)-PP complexes (left two panels). For δ-MnO_2, Mn(II) interacts with surface Mn(IV) sites to form Mn(III), which is then stabilized by PP (right panel). In this schematic, solid lines denote the presence of Mn ions on the mineral surface; dashed lines signify the formation of complexes. Circles with a fill denote Mn(III/IV) in its solid form, representing ions that are part of the mineral lattice.

Conversely, the circles without fill represent chemical species in the aqueous phase. All atoms are labeled, except for oxygen, which are depicted as small gray circles. Oxidized BPA derivatives (BPA_{ox}) are collectively represented. Note that the diagram is a simplified representation and not drawn to scale.

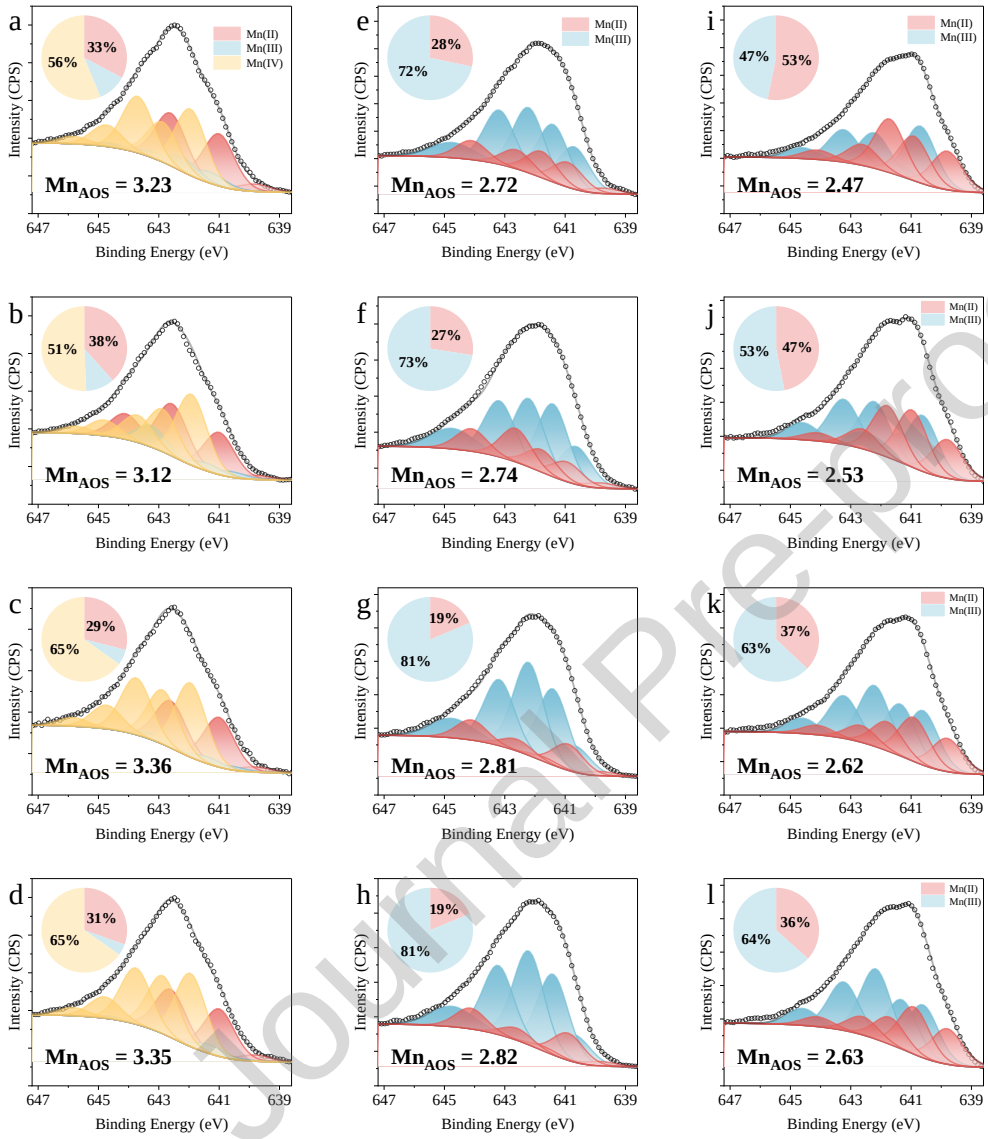

Figure 5. Mn $2p_{3/2}$ XPS spectra of varied Mn oxides with different PP concentrations at the end of the reaction. (a, b, c, d) With δ-MnO_2 and initial PP concentrations of 0, 200, 500, and 1000 μM. (e, f, g, h) With γ-MnOOH and initial PP concentrations of 0, 300, 1000, and 2000 μM. (i, j, k, l) With Mn_3O_4 and initial PP concentrations of 0, 200, 500, and 1000 μM. The legends for panels b, c, and d are the same as panel a; for panels f, g, and h, as panel e; and for panels j, k, and l, as panel i. For γ-MnOOH and Mn_3O_4, only Mn(II) and Mn(III) were fitted. Inserted pie charts show the relative fractions of Mn(II), Mn(III) and Mn(IV) based on the fitting results of the spectra (details in Table S1, S2, and S3).

Table 1. Summary of the Experimental Settings and Key Parameters

Exp[a]	PP (μM)	Mn(III) (μM)	δ-MnO_2 (g/L)	γ-MnOOH (g/L)	Mn_3O_4 (g/L)	$k_1(k_1')$[b,c] (μM^{-1} min^{-1})	k_2[b] (min^{-1})	k_3[b] (μM^{-1} min^{-1})	k_4[b] (μM^{-1} min^{-1})	$k_{obs}(k_{PP})$[d] (min^{-1})
1	600	100	-	-	-	-	-	N.A.[e]	-	-
2	1800	300	-	-	-	-	-	N.A.	-	-
3	3600	600	-	-	-	-	-	N.A.	-	-
4	2000	100	-	-	-	-	-	1.2×10^{-4}	-	-
5	6000	300	-	-	-	-	-	2.6×10^{-5}	-	-
6	12000	600	-	-	-	-	-	1.4×10^{-5}	-	-
7	0	-	0.1	-	-	6.1×10^{-5} (6.2×10^{-6})	/	/	4.8×10^{-4}	/
8	200	-	0.1	-	-	6.6×10^{-5} (7.0×10^{-6})	4.8×10^{-4}	2.0×10^{-4}	$<1.0\times10^{-9}$	2.4×10^{-4} (1.2×10^{-6})
9	500	-	0.1	-	-	6.5×10^{-5} (7.6×10^{-6})	1.8×10^{-3}	1.6×10^{-4}	$<1.0\times10^{-9}$	5.1×10^{-4} (1.0×10^{-6})
10	1000	-	0.1	-	-	6.4×10^{-5} (7.9×10^{-6})	8.0×10^{-3}	1.4×10^{-4}	$<1.0\times10^{-9}$	1.3×10^{-3} (1.3×10^{-6})
11	0	-	-	0.1	-	1.2×10^{-6}	$<1.0\times10^{-9}$	-	1.0×10^{-3}	/
12	300	-	-	0.1	-	1.8×10^{-6}	2.9×10^{-4}	1.1×10^{-6}	2.1×10^{-4}	8.1×10^{-5} (2.7×10^{-7})
13	1000	-	-	0.1	-	2.5×10^{-6}	5.5×10^{-4}	6.0×10^{-6}	1.4×10^{-4}	2.7×10^{-4} (2.7×10^{-7})
14	2000	-	-	0.1	-	2.0×10^{-6}	8.8×10^{-4}	4.6×10^{-6}	1.2×10^{-4}	6.2×10^{-4} (3.1×10^{-7})
15	0	-	-	-	0.1	$<1.0\times10^{-9}$	/	/	/	/
16	200	-	-	-	0.1	1.2×10^{-6}	3.6×10^{-4}	1.6×10^{-5}	9.0×10^{-4}	1.1×10^{-4} (5.3×10^{-7})
17	500	-	-	-	0.1	2.3×10^{-6}	4.5×10^{-4}	1.4×10^{-5}	5.3×10^{-4}	2.2×10^{-4} (4.4×10^{-7})
18	1000	-	-	-	0.1	3.0×10^{-6}	7.7×10^{-4}	8.9×10^{-6}	3.2×10^{-4}	4.9×10^{-4} (4.0×10^{-7})

[a]Experiments were performed in triplicate at pH 7.0 with 100 μM BPA. [b]The rate constants (k_1, k_2, k_3, and k_4) corresponding to the distinct reaction pathways of BPA degradation, as illustrated in Fig. 4(a-d), were determined by fitting the collected BPA and Mn(III) concentration data to the kinetic rate expressions, as described in the main text. PP concentration was not directly included in differential equations, but their impact was implied in the rate constants. [c]Two different reaction sites were proposed for δ-MnO_2, and k_1 denoted the reaction constant for >Mn(III), and k_1' for >Mn(IV). [d]The apparent dissolution rates of Mn oxides (k_{obs}) were calculated following a pseudo-first reaction order, where the concentrations of PP were not included. This rate constant is given for easy comparison with those observed in Mn oxides-BPA-PP systems. Inside the parentheses are the k_{PP} for Mn oxides dissolution following a second reaction order, with the unit of μM^{-1} min^{-1}. [e]N.A.: Not applicable. N.A. indicates cases where the low PP:Mn(III) ratio led to reaction rates that were too rapid for accurate linear fitting, even within the first two sampling intervals. To ensure precision, reaction rates in these instances were not presented.

Declaration of Competing Interest

☒ The authors declare that they have no known competing financial interests or personal relationships that could have appeared to influence the work reported in this paper.

Graphical abstract

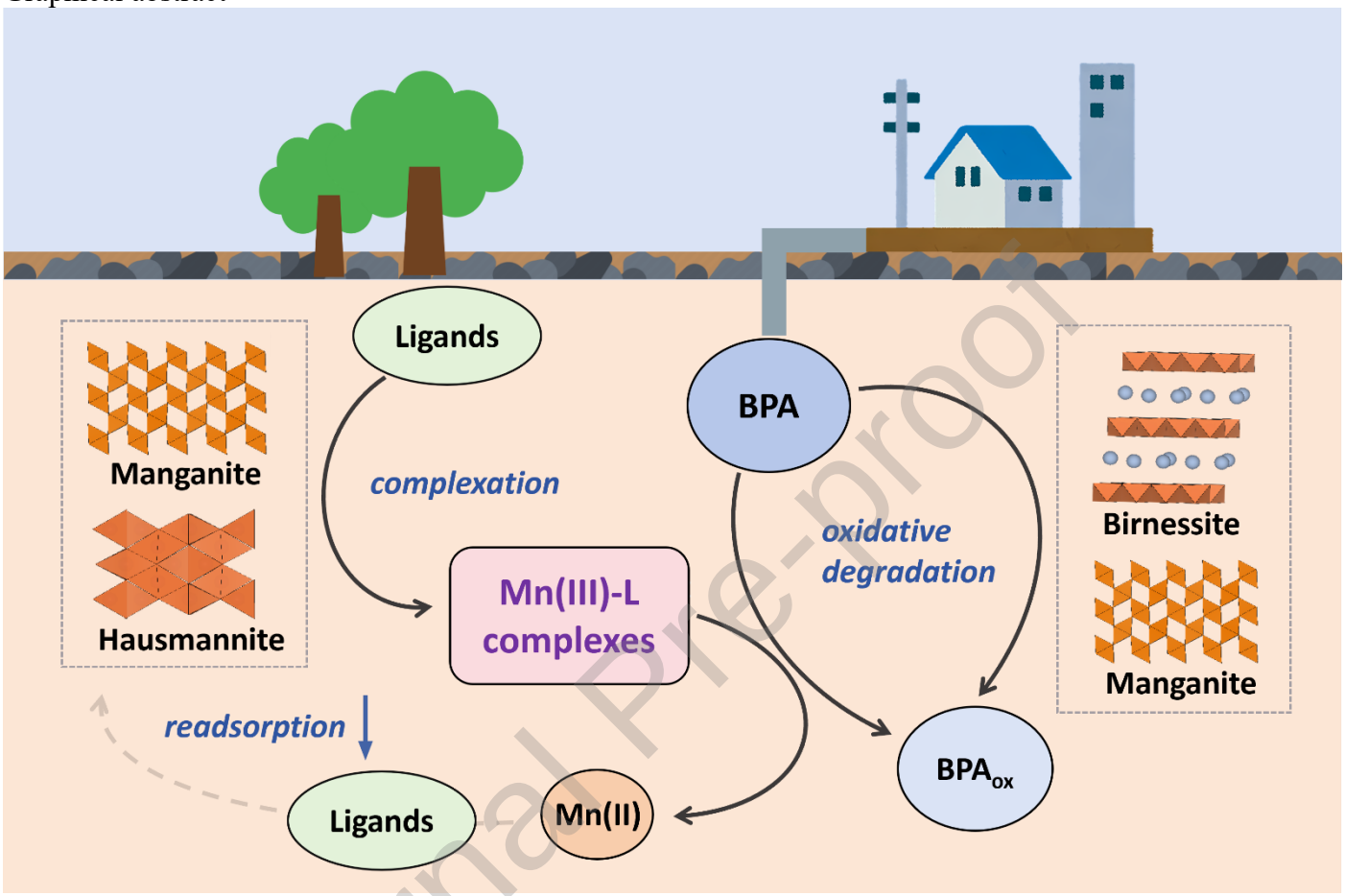

Highlights

- Crystal structures and ligand-to-metal ratios modulate Mn(III) reactivity in Mn oxides and dissolved species for Bisphenol A degradation.
- Pyrophosphate enhances Bisphenol A degradation by preventing mineral surface passivation.
- High PP concentrations hinder Bisphenol A binding to reactive Mn(III) in minerals and aqueous phases.